J Mater Sci (2007) 42:1594–1605
DOI 10.1007/s10853-006-0900-3

Characteristics of face-centered cubic metals processed by equal-channel angular pressing

N. Q. Chinh · J. Gubicza · T. G. Langdon

Received: 6 June 2006 / Accepted: 28 August 2006 / Published online: 9 January 2007
© Springer Science+Business Media, LLC 2006

Abstract This review surveys the characteristics of face-centered cubic (fcc) metals and alloys processed by equal-channel angular pressing (ECAP). The significance of the Hall–Petch relationship for ultrafine grained structures is examined and the dependence of the saturated stress obtained in ECAP on the absolute melting temperature is described and discussed. In addition, the flow processes at low temperatures in ultrafine-grained materials and the microstructural evolution of the dislocation densities and precipitates in some alloys of practical importance are also considered briefly.

Introduction

In modern materials science, one of the major requirements for advanced materials is attaining very high strength with a reasonable level of ductility. It is very important therefore to obtain a good understanding of the processes associated with the mechanisms both of strengthening and of plastic deformation. It is well known that these processes are strongly influenced by the composition and the crystalline grain size of the investigated materials. More than 50 years ago material researchers developed the so-called Hall–Petch equation [1, 2] which relates the yield stress, σ_y, necessary for yielding and plastic deformation to the grain size, d, through the expression

$$\sigma_y = \sigma_0 + K \cdot d^{-1/2} \tag{1}$$

where σ_0 is the friction stress and K is a positive material constant associated with the stress required to extend dislocation activity into adjacent grains. Equation (1) is very well established for materials having relatively large grain sizes ($d > 1$ μm) and it serves to demonstrate that the yield stress and then the strength increases as the grain size is decreased. In addition, it is also well known that the grain size plays an important role in superplastic flow where the main deformation mechanism is grain boundary sliding [3–6]. Under optimal conditions, the superplastic flow is often described by a constitutive equation of the form:

$$\dot{\varepsilon} = A \frac{D \cdot \mu \cdot b}{k \cdot T} \left(\frac{b}{d}\right)^p \left(\frac{\sigma}{\mu}\right)^q \tag{2}$$

where $\dot{\varepsilon}$ is the strain rate, D is the coefficient of grain boundary diffusion, μ is the shear modulus, b is the Burgers vector, k is the Boltzmann constant, T is the absolute temperature of testing, p is the grain size exponent, σ is the flow stress, q is the stress exponent and A is a dimensionless constant. On the basis of this constitutive law, it is reasonable to expect that a

N. Q. Chinh (✉) · J. Gubicza
Department of Materials Physics, Eötvös University, Budapest, Pázmány P. sétány 1/A, Budapest 1117, Hungary
e-mail: chinh@metal.elte.hu

T. G. Langdon
Departments of Aerospace & Mechanical Engineering and Materials Science, University of Southern California, Los Angeles, CA 90089-1453, USA

T. G. Langdon
Materials Research Group, School of Engineering Sciences, University of Southampton, Southampton SO17 1BJ, UK

decrease of grain size will lead to an increase in the occurrence of superplasticity at relatively low temperatures and/or higher testing strain rates.

The significance of both Eqs. (1) and (2) is an important reason for the sustained efforts to obtain finer grain structures in different metals and alloys. It is well known that bulk fine-grained structures can be attained by applying severe plastic deformation when the large numbers of dislocations introduced during deformation become progressively arranged into high-angle boundaries and thereby lead to an ultrafine-grained structure. In the last decade, several methods [7] such as equal-channel angular pressing (ECAP), high-pressure torsion (HPT), accumulative roll-bonding (ARB), multi-directional forging (MDF), cyclic extrusion and compression (CEC) and twist extrusion (TE) were developed for introducing severe plastic deformation into metals and alloys. These procedures are quite different both in the physical principle of their operations and in the sizes of the workable pieces. Considering both the advantages of the processing methods and the fundamental sizes of the useable samples, ECAP [8–11] may be regarded as the most important processing tool for grain refinement. Applying this method, ultrafine (sub-micrometer) microstructures have been obtained in several fcc metals and their alloys, as documented in Table 1, and these processed microstructures have important characteristics for use in many practical applications.

The objective of this paper is to summarize the effect of severe plastic deformation introduced by ECAP on fcc metals and alloys. For pure metals, the grain size, d, obtained by ECAP and the corresponding saturation strength, σ_{sat}, are described and discussed by using the basic elastic and thermodynamic characteristics of the metals through the shear modulus, μ, and the absolute melting temperature, T_m. Furthermore, the flow processes at low temperatures ($T < 0.5T_m$) in ultrafine-grained materials, as well as the evolution of microstructural features such as dislocation densities and precipitation in some alloys of practical importance, are also reported.

Table 1 Examples of grain sizes of some fcc metals and alloys processed by ECAP

Material	Grain size, d (nm)	Magnitude of Burgers vector, b (nm)
Al	1100 [12], 1300 [13]	0.286
Cu	270 [14], 300 [15], 420 [16], 500 [17]	0.255
Ni	200 [18], 300 [19]	0.249
Al–1% Mg	450 [13]	0.286
Al–3% Mg	300 [13]	0.286
Al–3% Mg–0.2% Sc	200 [20, 21]	0.286

The basic relationships and deformation mechanisms in fcc metals processed by ECAP

Correlation between normalized saturation strength and the absolute melting point

A recent report [22] described the homogenous plastic deformation of pure Al and Cu deformed at room temperature and demonstrated that the macroscopic stress–strain (σ–ε) relationship may be fitted by the constitutive equation:

$$\sigma = \sigma_0 + \sigma_1\left[1 - \exp\left(\frac{-\varepsilon}{\varepsilon_c}\right)^n\right], \quad (3)$$

where σ_0, σ_1, ε_c and the exponent n are constant fitting parameters and the strain ε is taken as the absolute amount of strain relative to the annealed state. It can be seen that the constitutive equation (3) is a generalized relationship including the main features of both the more conventional Hollomon-type power-law [23] and the Voce-type exponential equation [24]. By incorporating the behavior of samples severely deformed by applying ECAP, it was noted that the new constitutive relationship shown in Eq. (3) applies over a wide range of strains. A recent analysis demonstrated that this equation also describes the macroscopic stress–strain relationship of Au and Ni metals. Considering the development properties of Eq. (3), it can be seen that at high strains (large ε) the flow stress, σ, tends to the value of the saturation stress, $\sigma_{sat} = \sigma_0 + \sigma_1$. In practice, this state corresponds to severe plastic deformation applied, for example, by ECAP. The validity of Eq. (3) is confirmed also by the fact that at high strains the value of the saturation stress, σ_{sat}, agrees well with the flow stress obtained in ECAP samples for several fcc metals, as shown in Table 2. It should be noted also that the constant, σ_0, in Eq. (3), is practically the 0.2% proof stress of the annealed state representing the onset of any plastic deformation: thus, the experimental values of σ_0 are 20, 27, 35 and 60 MPa for Al, Au, Cu and Ni, respectively. Furthermore, Eq. (3) reflects also the well-established Taylor relationship

$$\sigma = \sigma_0 + \sigma_p, \quad (4)$$

Table 2 The saturation yield stress determined experimentally after ECAP and the equivalent saturation stress obtained from fitting Eq. (1) for fcc metals

Metal	Saturation stress, σ_{sat} (MPa)	
	After ECAP	$\sigma_{sat} = \sigma_0 + \sigma_1$ fitted by Eq. (3)
Al	120 [14] 122 [22]	119 [22]
Au	245 [25]	237 [unpublished]
Cu	395 [14] 380 [26] 390 [27]	383 [22]
Ni	–	1138 [unpublished]

in which the stress, σ_p, during plastic deformation, is related to the average dislocation density ρ through the expression

$$\sigma_p = \alpha \cdot M \cdot \mu \cdot b \cdot \sqrt{\rho} \tag{5}$$

where α is a geometrical constant ($\alpha \approx 0.33$) and M is the Taylor factor ($M = 3$ for untextured polycrystalline materials).

Considering the saturation stress, the value of $\sigma_{p,max} = \sigma_{sat} - \sigma_0$ characterizes the maximum hardening achieved by SPD. This quantity is naturally determined by a dynamic equilibrium between the formation and annihilation of dislocations. As the rate of dynamic recovery is influenced by the homologous temperature of deformation, the valus of $\sigma_{p,max}$ obtained at room temperature (RT = 293 K) for different fcc metals are expected to depend on the absolute melting temperature, T_m.

Figure 1 shows a logarithmic plot of the dimensionless shear modulus-normalized strength, $\sigma_{p,max}/\mu$, obtained by ECAP at room temperature versus the melting point for Al, Au, Cu and Ni. The linear

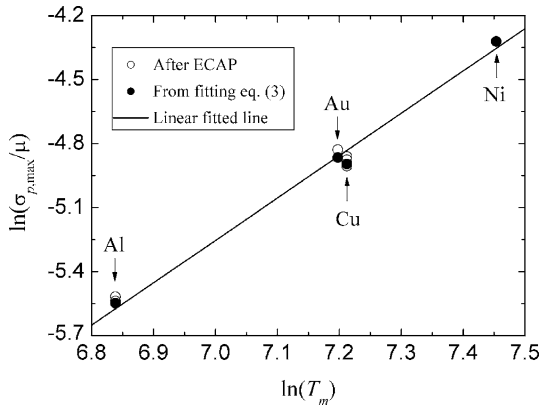

Fig. 1 The maximum yield strength, $\sigma_{p,max}/\mu$, obtained by ECAP versus the absolute melting temperature, T_m, for fcc metals

relationship in Fig. 1 suggests that, at a given processing speed and hydrostatic pressure, the following simple relationship may apply:

$$\frac{\sigma_{p,max}}{\mu} = A \cdot T_m^2 \tag{6}$$

where A is a universal constant for all of the investigated fcc metals and with a value of $A \approx 3.13 \times 10^{-9}$ K^{-2}. This experimental relationship shows that the shear modulus-normalized saturated strength, $\sigma_{p,max}/\mu$, is an important macroscopic feature of different fcc metals severely deformed by ECAP at room temperature and, in addition, it can be scaled through a simple relationship involving the absolute melting point.

The existence of Eq. (6) reveals that, according to Eq. (5), the saturated dislocation density, ρ_{max}, is an important microscopic quantity which, when obtained by ECAP, depends only on the melting point of the material. Qualitatively, if it is accepted that the annihilation of dislocations is controlled by vacancy diffusion, the saturation dislocation density at room temperature is determined by the activation energy, Q_{self}, of lattice self-diffusion. As Q_{self} for fcc metals is proportional to the melting point [28], the maximum dislocation density at RT depends only on the melting temperature. The assumption that the dislocation annihilation is controlled by vacancy diffusion at room temperature may be realistic for ECAP-processed ultrafine-grained metals by noting that a large fraction of vacancies formed during SPD can easily migrate in the material as a result of the high volume fraction of grain boundaries in nanocrystalline materials. Thus, it was found that diffusion in these structures is faster than in coarse-grained specimens by up to a factor of ~10^{10}–10^{20} [29]. Moreover, the movement of vacancies is further facilitated by the high value of the dislocation density as vacancies move easily in the cores of the dislocations.

The Hall–Petch relationship for ultrafine-grained fcc metals

As already mentioned, the original Hall–Petch relationship in general works very well for polycrystalline materials having grain sizes larger than $d \approx 1$ μm. Results from recent investigations, however, show evidence that this relationship may not hold when testing with ultrafine grain sizes. On the one hand some data are possibly consistent with Eq. (1) although with a lower value of K than for larger grain sizes [30–34] and on the other hand some data exhibit an apparent

decrease in yield stress with decreasing grain size indicating a softening effect at very fine grain sizes [32, 34–37]. While the current models [32, 34, 35, 38–41] explaining the softening process are quite different and inconclusive, the Hall–Petch type of behavior is basically interpreted by the concept of dislocation pile-ups formed at grain boundaries [34, 42–44]. In this context, it is considered that dislocations are generated by Frank-Read sources and then arrested at the grain boundaries of grains having a size of d. At the proper effective shear stress, τ_e, the pile-up of these dislocations then results in a maximum normalized dimensionless stress, σ_{pile}, having a value equal to [42]:

$$\sigma_{pile} = \pi(1-\nu)\left(\frac{d}{b}\right)\left(\frac{\tau_e}{\mu}\right)^2 \tag{7}$$

for a neighbor grain, where ν is the Poisson number (equal to about 1/3 for all fcc metals). In the case of large grain sizes, it can be assumed that macroscopic plastic deformation may be observed if multi-slip systems are activated at a constant value, C_1 of σ_{pile}, which leads to

$$\frac{\tau_e}{\mu} = \sqrt{\frac{C_1}{\pi(1-\nu)}}\left(\frac{d}{b}\right)^{-1/2}, \tag{8}$$

where this is the conventional Hall–Petch relation for a normalized stress and grain size.

For very fine grain sizes ($d < 100$ nm), the numbers of dislocations in the pile-ups tend to one giving pile-up breakdown [34, 44], and the value of σ_{pile} is now proportional to the normalized shear stress so that

$$\sigma_{pile} = C_2\left(\frac{\tau_e}{\mu}\right), \tag{9}$$

where C_2 is also a constant. Combining Eq. (9) with Eq. (7) leads to.

$$\frac{\tau_e}{\mu} = \frac{C_2}{\pi(1-\nu)}\left(\frac{d}{b}\right)^{-1}. \tag{10}$$

According to the experimental data, which show rather a monotonously changing slope of the Hall–Petch relation obtained for a wide range of grain sizes [34, 44], it is reasonable to suppose that in general the value of σ_{pile} is a power law function of the normalized effective shear stress of the form

$$\sigma_{pile} = C_3\left(\frac{\tau_e}{\mu}\right)^{\beta}, \tag{11}$$

where C_3 and β are constants depending on the range of grain size: thus, for large grain sizes, $d > 1000$ nm, $C_3 = C_1$ with $\beta = 0$, and for very fine grain sizes, $d < 100$ nm, $C_3 = C_2$ with $\beta = 1$. In the middle range of grain sizes, in the sub-micrometer grain sizes for fcc metals processed by ECAP as documented in Table 1, a value of β is expected between 0 and 1. It should be noted that the grain sizes measured in ECAP Cu are very scattered in Table 1, probably because of the advent of dynamic recovery [45]. Taking into account Eqs. (7) and (11) and using the usual yield stress, σ_y, the Hall–Petch relation can be expressed in the form of

$$\frac{\sigma_y}{\mu} = \frac{\sigma_0}{\mu} + K^*\left(\frac{d}{b}\right)^{\lambda}, \tag{12}$$

where K^* is a constant, $\lambda = -1/(2-\beta)$ and $-1/2 \geq \lambda \geq -1$.

Taking the saturated stress, σ_{sat}, given in Table 2 as the yield stress for ECAP-pressed pure metals and Al–Mg alloys [13], the data analysis shown in Fig. 2 implies that for the ultrafine grain sizes obtained in fcc metals and solid solutions the value of λ is about –0.77 so that the Hall–Petch equation (1) is modified to the form

$$\frac{\sigma_y}{\mu} = \frac{\sigma_0}{\mu} + K^*\left(\frac{d}{b}\right)^{-0.77}. \tag{13}$$

It should be mentioned that in this case the value of the parameter β in Eq. (11) is 0.70, indicating an intermediate condition between those of large and very fine grains characterized by the activation of totally multi-slip or single slip, respectively, inside the individual grains. The main Hall–Petch behavior is summarized in Table 3 as a function of the grain size.

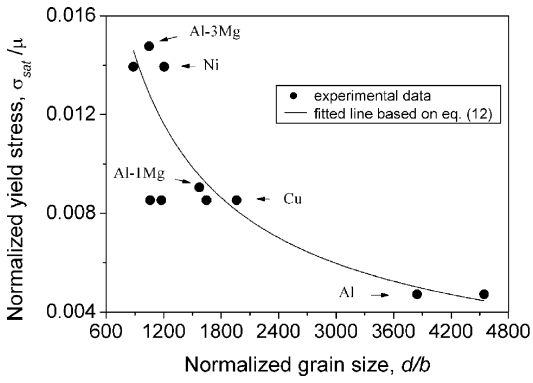

Fig. 2 The normalized yield stress, σ_{sat}/μ, of ECAP metals and alloys versus the normalized grain size, d/b

Table 3 The main Hall–Petch behavior in the different ranges of grain size

Range of grain size, d	Hall–Petch behavior $\frac{\sigma_y}{\mu} = c_1 + c_2\left(\frac{d}{b}\right)^{\lambda}$
$d > 1000$ nm, large grains	$c_1 > 0$, $c_2 > 0$, $\lambda = -0.5$
$d \approx 100 \div 1000$ nm, ultra-fine grains	$c_1 > 0$, $c_2 > 0$, $\lambda \approx -0.77$ ($-0.5 > \lambda > -1$)
$d \approx 5 \div 100$ *nm*, very fine grains	$c_1 > 0$, $c_2 > 0$, $\lambda = -1$
$d < 5$ nm, nano-grains	$c_2 < 0$ (softening)

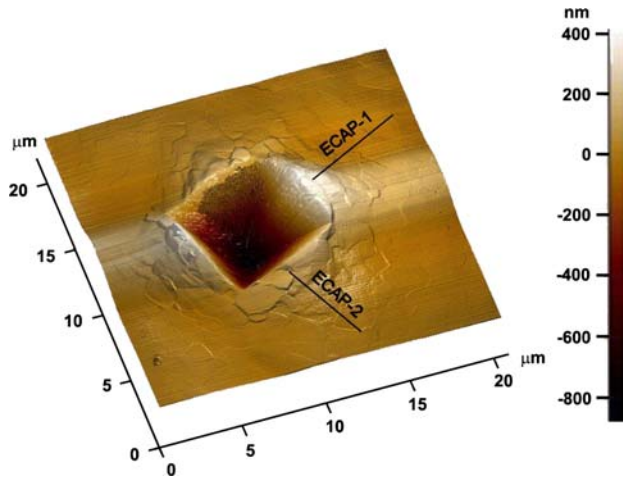

Fig. 3 An AFM micrograph of the surface of an ECAP Al sample deformed by indentation using a Vickers indenter [58]

Flow processes in ultrafine-grained structures: the role of grain boundary sliding

When pure metals having conventional grain sizes of $d > 10$ μm are deformed in tensile or compression tests at low temperatures ($T < 0.5T_m$), the flow stress, σ, in general monotonously increases with increasing strain, ε. Most investigations of these relatively coarse-grain materials have been restricted to an examination of the strain hardening behavior in the low temperature regime or creep properties only in the high temperature regime ($T > 0.5T_m$). As a consequence, the flow behavior at low temperatures is invariably focused exclusively on the characteristics of the region of work-hardening and the nature of the stress–strain (σ–ε) relationship in the different regions of strain [23, 24, 46–48]. Recently, applying Eq. (1) for high purity aluminum and copper, it was shown that it may be feasible to develop an alternative analytical interpretation for the flow processes in fcc metals by using the new constitutive equation (3) over a very wide range of testing temperatures [49, 50].

In the case of ECAP samples, which have ultrafine-grained microstructures, several experimental data [22, 34, 50, 51] show that the flow process at low temperatures can be described rather by steady-state creep with practically zero work-hardening. Recent results [49, 50] obtained on pure Al demonstrated that, whereas at high temperatures ($T > 0.5T_m$) the rate of steady-state creep is controlled by diffusion through the crystalline lattice, in the low temperature region ($T > 0.5T_m$) grain boundary diffusion becomes a significant factor in determining the rate of steady-state flow. Furthermore, it appears that in the ultrafine-grained Al deformed at relatively low temperatures, flow occurs with a significant contribution from a grain boundary process such as grain boundary sliding. This explanation is also consistent with the reasonably constant microstructures that are observed in pure Al and aluminum-based alloys after ECAP pressing [13, 52].

The occurrence of grain boundary sliding at low temperatures has been predicted in the modeling of nanocrystalline solids using three-dimensional molecular dynamics computer simulations [53, 54] and several experimental investigations [55–57] also suggest this mechanism as a viable deformation process. Although there have been some attempts to show localization of plastic flow in the grain boundary regions [55–57], convincing direct experimental evidence for the occurrence of grain boundary sliding in ultrafine-grained materials was reported only very recently [58] by employing depth sensing indentation (DSI) and atomic force microscopy (AFM).

Using AFM, the mechanism of grain boundary sliding was evaluated in an ECAP Al sample using indentation with a Vickers indenter as shown in Fig. 3. It can be seen that around the Vickers pattern there is a rumpling on the surface, which corresponds to the displacements of grains relative to each other within the ultrafine-grained matrix, demonstrating clearly the occurrence of grain boundary sliding as a significant mechanism for deformation in the ECAP Al. The supplemented height profiles shown in Fig. 4 demonstrate that adjacent grains may slide up to ~30 nm over each other. It was also shown that there was a significant contribution of sliding to the total strain in the ECAP sample, with a measured sliding contribution of up to ~70% [58]. This estimate is consistent with the proposal that grain boundary sliding occurs relatively easily at low homologous temperatures at the non-equilibrium boundaries introduced into materials processed by severe plastic deformation [27].

It should be noted that the ease of grain boundary sliding is consistent with the superplastic ductilities of

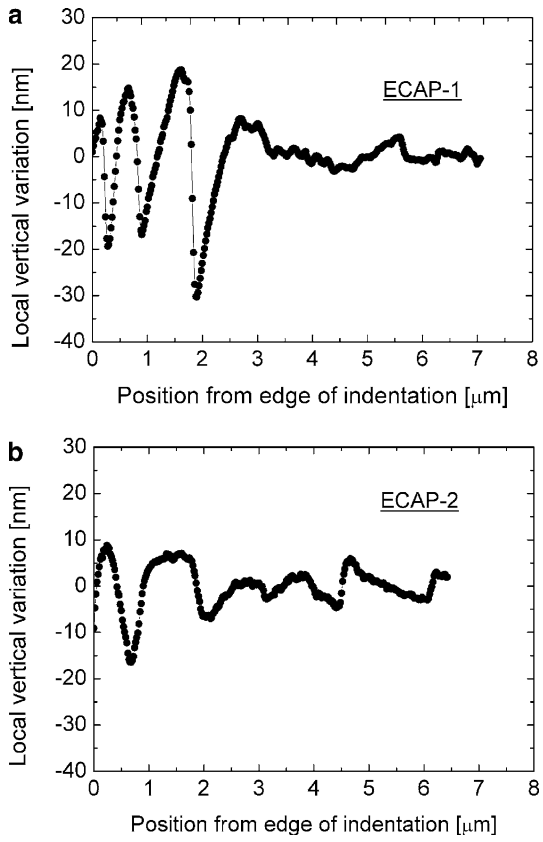

Fig. 4 Plots of the local vertical variations against the position from the edge of the Vickers pattern for the ECAP condition shown in Fig. 3 for paths 1 (**a**) and 2 (**b**), respectively [58]

several ultrafine-grained materials deformed at exceptionally high strain rates and unusually low temperatures [10, 11, 21]. Applying the ECAP processing technique, ultrafine-grained structures were introduced in an Al–3% Mg–0.2% Sc alloy [21] which was superplastically deformed with elongations up to >1000% at strain rates up to 10^{-1} s^{-1}. The essential variation of the conditions for superplastic deformation, including decreasing temperature and increasing strain rate, has a significant practical importance in industrial production processes. Another extraordinary effect of the ultra-fine grained structures manifests itself in the occurrence of Portevin–Le Chatelier (PLC) type plastic instabilities [59] which are often observed in coarse-grained Al–Mg solid solutions during depth-sensing indentation tests [60–64]. Recently, it was shown that the occurrence and development of instability indentation steps in the ultrafine-grained Al–3% Mg alloy depends strongly on the indentation size [59]. Under certain conditions, dislocation motion within the grains makes only a limited contribution to the plastic deformation and instead grain boundary processes become rate-controlling leading to the disappearance of the PLC effect.

Microstructure and mechanical behavior of ECAP-processed solid solutions

Evolution of microstructure during ECAP

To understand the mechanical behavior of ECAP-processed solid solutions, a study of the effect of alloying on microstructural evolution is essential. It was found that the dislocation density increases with increasing numbers of ECAP passes and saturates after ~4–8 passes for both pure fcc metals and solid solutions [45, 65–71]. As an example, the dislocation density versus the imposed strain for an Al–3% Mg specimen is plotted in Fig. 5 [65]. The saturation values correspond to the dynamic equilibrium state between the formation and annihilation of dislocations. The maximum dislocation densities at room temperature for different fcc materials are listed in Table 4. The effect of Mg solute atoms on the evolution of the microstructure in Al during ECAP is shown in Fig. 6 where the dislocation density is plotted as a function of the Mg content after 8 ECAP passes [71]. The saturation value of the dislocation density is higher for a higher Mg concentration as the Mg atoms hinder the annihilation of dislocations. For example, in the Al–3% Mg alloy the maximum dislocation density is approximately 13 times higher than for pure Al [65]. As grain refinement in SPD metals occurs by the rearrangement of dislocations into cell boundaries, the higher dislocation density results in a decrease of grain size for higher Mg concentrations as shown in Fig. 6 and demonstrated earlier in Table 1.

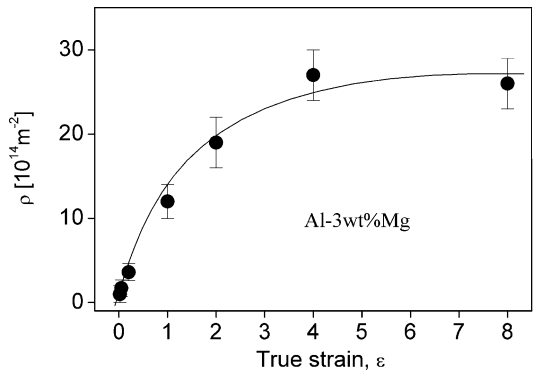

Fig. 5 The dislocation density for Al–3 wt.% Mg processed by ECAP as a function of the imposed strain

Table 4 The saturation value of the dislocation density (ρ) obtained by X-ray line profile analysis for different fcc metals and alloys processed by SPD

Material	ρ (10^{14} m^{-2})
Al	1.8 [65]
Cu	26 [67, 71]
Au	17 [unpublished]
Ni	25 [18, 72]
Al–1%Mg	3.9 [71]
Al–3%Mg	23 [65, 71]
Al 6082	5.4 [73]
Al–Zn–Mg–Zr	3.2 [74]
Al–Zn–Mg–Cu	3.4 [74]

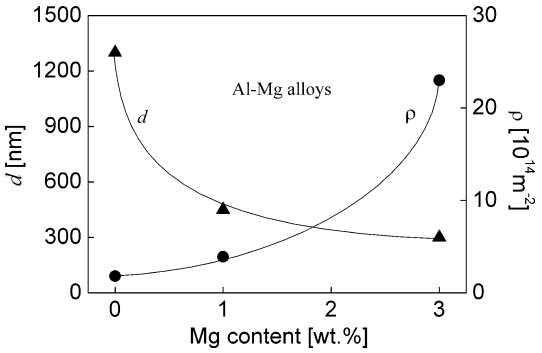

Fig. 6 The saturation value of the grain size, d, and the dislocation density, ρ, as a function of the Mg concentration in Al

The relation between the dislocation density and the saturation yield stress: the Taylor relationship over a wide range of strain

When considering the strength of an ultrafine-grained alloy, different strengthening mechanisms must be examined. Specifically, these are (i) the work-hardening process, in terms of the interaction between dislocations in the grain interiors of the matrix, (ii) the Hall–Petch effect, in terms of the interactions between dislocations and grain boundaries, (iii) the solid solution hardening and (iv) the precipitation strengthening [75]. The first three effects occur if the alloy is a solid solution while the fourth effect should be taken into account additionally if the material contains precipitates. The yield strength corresponding to the interaction between dislocations can be calculated from the total dislocation density using the Taylor equation given in Eqs. (4) and (5). In Fig. 7, the yield strength, σ_{measured}, measured by mechanical tests versus the values calculated, σ_{Taylor}, from the dislocation density determined by X-ray line profile analysis are plotted for different fcc metals and solid solutions

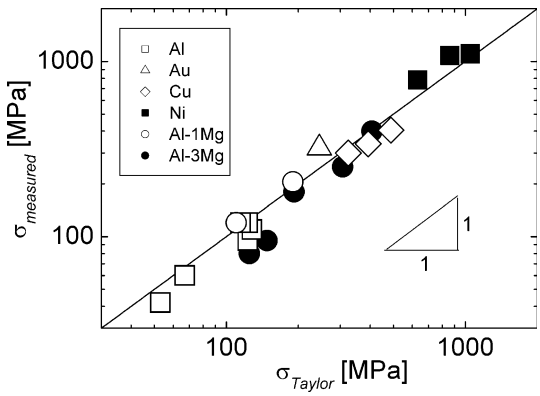

Fig. 7 The yield strength. σ_{measured}, measured by mechanical testing versus the values, σ_{Taylor}, calculated from the dislocation density according to Eq. 5 for different fcc pure metals and solid solutions

deformed at different strains from $\varepsilon \approx 0.05$ up to 14. The values of σ_{measured} were determined by compression, tension or Vickers hardness measurements. It is apparent that the yield strength measured by mechanical tests are in relatively good agreement with the values calculated according to the Taylor equation, indicating that in fcc metals processed by SPD the strength is basically determined by the interactions between dislocations.

This result suggests that for ultrafine-grained metals and solid solutions processed by SPD the effect on the strength between the dislocations in work-hardening, the grain boundaries in the Hall–Petch relationship and the solute atoms in solid solution hardening can be incorporated into the average dislocation density, ρ. For the effect of the grain boundaries, this observation can be explained by the fact that in materials processed by SPD the grain refinement occurs by the arrangement of dislocations into subgrain-boundaries and/or dislocation walls. Consequently, the majority of boundaries consists of dislocations and the effect of subgrain/grain boundaries on dislocation motion can be regarded as the interaction between dislocations [76]. Concerning the solid solution strengthening, the solute atoms may increase the strength in two ways: (i) directly by pinning the dislocations and impeding their motion in a solute-dislocation interaction and (ii) indirectly by hindering the annihilation of dislocations during deformation, leading to an increase in the dislocation density in a dislocation–dislocation interaction. For severely deformed metals where the dislocation density is relatively high, the latter factor is dominant so that the hardening effect of the solute atoms is manifested basically in the higher dislocation density.

Behavior of precipitation-hardened fcc alloys

Superplastic behavior of ECAP processed alloys

The influence of ECAP on the flow behavior of precipitation-hardened alloys was demonstrated with a commercial spray-cast Al-7034 alloy having a chemical composition (in wt.%) of 11.5% Zn–2.5% Mg–0.9% Cu–0.2% Zr with the balance of Al [77, 78]. The initial grain size of 2.1 μm was reduced to 300 nm after 6 ECAP passes at 473 K. An as-received specimen and a sample processed by six passes were subjected to tensile testing at 623 K at strain rates between 10^{-3} and 10^{-1} s^{-1}. The elongations in the as-received condition were in the range of 150–300%. The ECAP-processed specimen showed higher elongation for any strain rate and the maximum elongation was higher than 1000% at strain rates in the vicinity of ~10^{-2} s^{-1} [79]. In tensile testing at 673 K, the as-received alloy showed reasonable ductility with elongations in the range from ~400% to 600%. This relatively high ductility is due to the very small initial grain size after spray-casting. Similar elongations were evident also after 1 pass of ECAP but for six and eight passes the elongations increased and reached maximums values higher than 1000% at strain rates of 1.0×10^{-2} to 3.0×10^{-2} s^{-1} [80–83]. The maximum elongation occurred at higher strain rates with an increase in the number of ECAP passes which was attributed to the higher fraction of high-angle grain boundaries. As superplastic deformation occurs through grain boundary sliding that requires boundaries having high angles of misorientation, the increasing fraction of high-angle boundaries leads to easier sliding. The increase in the ductility with an increase in the number of ECAP passes was also observed in an Al–5.5% Mg–2.2% Li–1.2% Zr alloy processed by ECAP at 673 K [84], in an Al–3% Mg–0.2% Sc alloy processed by ECAP at 673 K [85] and in an Al-6016 alloy processed by ECAP at 473 K [86]. The very high elongations for the ECAP-processed samples is due to the ultrafine-grained microstructure which was retained in these alloys even at high testing temperatures because of the presence of precipitates which impeded grain boundary mobility. For example, the stabilization effect of $Al_3(Zr_xSc_{1-x})$ precipitates on the fine-grained microstructure was observed in ECAP-processed Al–Mg alloys with Sc and Zr additions, leading to superplastic deformation at 773 K and at strain rates in the vicinity of ~10^{-2} s^{-1} [87].

The influence of ECAP on the precipitation processes

The ECAP process has a significant effect on the size and shape of precipitates. If the ECAP procedure is conducted on precipitation-hardened alloys, the rod-like precipitates may become fragmented into smaller spherical particles. An example of this effect was demonstrated for the Al-7034 alloy where fragmentation of the rod-like $MgZn_2$ particles was significant even after the first ECAP pass at 473 K and additional breaking occurred during subsequent passes [78]. Tensile and creep tests were also conducted on the Al-7034 specimens cut from the unpressed and as-received bars and from billets processed by ECAP. In creep testing at 473 K, the creep rates recorded for the ECAP samples were about two orders of magnitude faster than for the as-received alloy at the same stress value [80]. There are three reasons for the occurrence of faster creep rates in the ECAP alloy. First, the grain size is reduced by ECAP and this leads to faster rates through Eq. (2). Second, the ECAP material contains a higher dislocation density because of the intense straining imposed during ECAP. Third, there is easier deformation within the grains after ECAP because of the fragmentation and removal of the long rod-like $MgZn_2$ precipitates whereas, by contrast, these precipitates are present in the as-received alloy and constitute significant obstacles to dislocation movement. The fragmentation and partial dissolution of precipitates during ECAP was observed also in an Al–1.7 at.% Cu alloy [88], an Al–5 wt.% Ti alloy [89] and in a Cu–Cr–Zr alloy [90]. The breaking and dissolution of precipitates leads to a reduction in hardness in the Al–Ti alloy [89] and a reduction of stress amplitude in the course of fatigue of the Cu–Cr–Zr alloy [90].

The influence of ECAP on the formation of precipitates in supersaturated Al–Zn–Mg alloys has been studied. For this purpose, supersaturated Al–4.8Zn–1.2Mg–0.14Zr and Al–5.7Zn–1.9Mg–0.35Cu (wt.%) alloys were processed for 8 ECAP passes at 473 K [74]. Owing to the relatively high temperature of ECAP, the $MgZn_2$ precipitates (the η phase) were formed from the supersaturated solid solution: this is shown in the X-ray diffractogram in Fig. 8a. The η precipitates develop usually during ageing from the Guinier–Preston (GP) zones through the intermediate η' phase. To study the effect of ECAP on the development of the microstructure at high temperatures, additional specimens were aged at 473 K for 30 min, which is equal approximately to the duration of the 8 ECAP passes. The reflections of $MgZn_2$

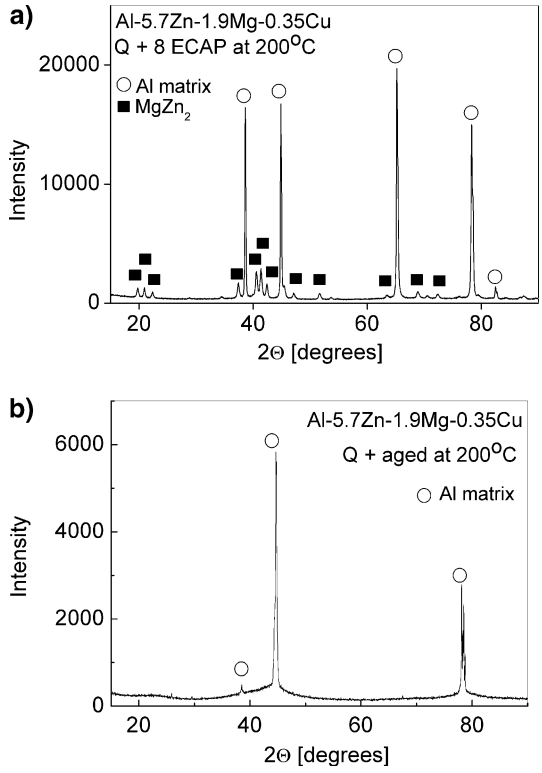

Fig. 8 The X-ray diffractograms taken on the Al–5.7Zn–1.9Mg–0.35Cu specimens (**a**) quenched and processed by ECAP at 473 K and (**b**) quenched and aged at 473 K for 30 min

precipitates cannot be observed on the X-ray diffractogram taken on the aged Al–5.7Zn–1.9Mg–0.35 Cu sample as shown in Fig. 8b. Comparing the diffractograms in Figs. 8a and 8b, it is concluded that the formation of the η phase was promoted by SPD. For the Al–4.8Zn–1.2Mg–0.14Zr specimen, the same phenomenon was observed although very weak reflections of $MgZn_2$ appear. This observation is supported by the TEM micrographs in Figs. 9 and 10 where, respectively, the microstructures of the ECAP-processed and aged Al–4.8Zn–1.2Mg–0.14Zr and Al–5.7Zn–1.9Mg–0.35Cu alloys are presented. Figure 10 shows that $MgZn_2$ precipitates exist also in the Al–5.7Zn–1.9Mg–0.35Cu alloy but the relative fraction of these particles is very low which explains the missing of $MgZn_2$ reflections in the diffractogram of Fig. 8a. The promoting effect of ECAP on the formation of precipitates can be explained by the high dislocation density since dislocations readily act as nucleation sites for η particles. Differential scanning calorimetry (DSC) measurements have also shown in the Al-7034 alloy that ECAP promotes the formation of η precipitates as the endothermic peak related to the dissolution of GP zones is missing from the DSC curve of ECAP-processed Al–Zn–Mg alloys while this peak exists for the aged specimens [91]. A DSC investigation of an Al-7075 alloy also indicated that the ECAP process not only accelerated the phase precipitations but also led to no change in the sequence of phase precipitation [92].

Strengthening in the precipitate-hardened ECAP alloys

Considering the strength of particle-hardened ultrafine-grained alloys, and assuming the additivity of the different strengthening contributions, the yield strength may be expressed by the following relationship [93]:

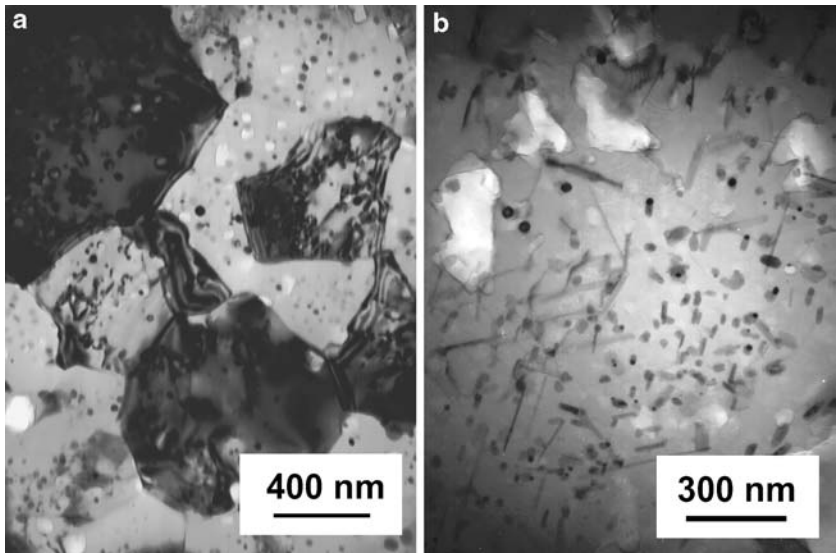

Fig. 9 TEM images obtained on the Al–4.8Zn–1.2Mg–0.14Zr alloy (**a**) quenched and processed by ECAP at 473 K and (**b**) quenched and aged at 473 K for 30 min

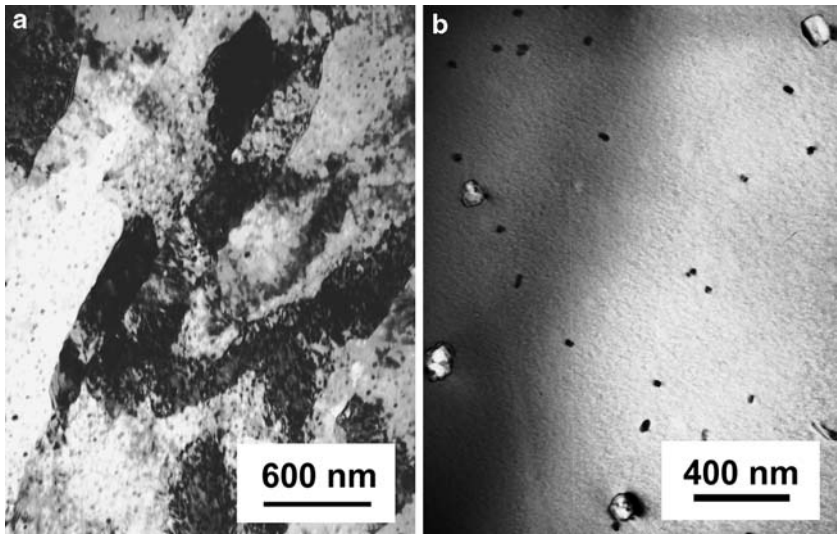

Fig. 10 TEM images taken on the Al–5.7Zn–1.9Mg–0.35Cu specimens (**a**) quenched and processed by ECAP at 473 K and (**b**) quenched and aged at 473 K for 30 min

$$\sigma_y = \sigma_0 + \alpha M \mu b \rho^{1/2} + 0.85M \frac{\mu b \ln(x/b)}{2\pi(L-x)}, \quad (14)$$

where x is the average size of precipitates and L is the average distance between them. The different contributions to yield strength were calculated from Eq. (14) using the values of L and x obtained from TEM micrographs and the dislocation density determined by X-ray line profile analysis. The average size of the precipitates in the Al–4.8Zn–1.2Mg–0.14Zr and Al–5.7Zn–1.9Mg–0.35Cu alloys obtained from the images of Figs. 9a and 10a were 30 and 20 nm, respectively. The average distance, L, between the precipitates was approximately 120 nm in the Al–4.8Zn–1.2Mg–0.14Zr alloy and 80 nm in the Al–5.7Zn–1.9Mg–0.35Cu alloy. The value of σ_0 was taken as 20 MPa measured for pure Al [22] because the lattice parameter of the matrix obtained from the X-ray diffractograms agrees with the value for pure Al within the experimental error. The dislocation densities due to ECAP at a temperature of 473 K were 3.2×10^{14} and 3.4×10^{14} m^{-2} for the Al–4.8Zn–1.2Mg–0.14Zr alloy and the Al–5.7Zn–1.9Mg–0.35Cu alloy, respectively. The strength contributions originating from the dislocation density given by the second term in Eq. (14) were 133 and 137 MPa for Al–4.8Zn–1.2Mg–0.14Zr and Al–5.7Zn–1.9Mg–0.35Cu, respectively, as the dislocation densities in the two matrices are very close to each other. The third term in Eq. (14) caused by the dislocation–precipitation interaction gave 156 MPa and 214 MPa for Al–4.8Zn–1.2Mg–0.14Zr and Al–5.7Zn–1.9Mg–0.35Cu, respectively, where the difference between the two values was due to the different size and dispersion of precipitates. Thus, the smaller particles with a more dense distribution lead to a higher strength for the Al–5.7Zn–1.9Mg–0.35Cu alloy. Finally, the sum of the three components leads to estimated total strengths of 309 MPa and 371 MPa which are in good agreement with the values of 290 MPa and 380 MPa determined by mechanical testing for the Al–4.8Zn–1.2Mg–0.14Zr alloy and the Al–5.7Zn–1.9Mg–0.35Cu alloy, respectively.

Summary and conclusions

(1) It is shown that the shear modulus-normalized saturated strength, $\sigma_{p,\max}/\mu$, of different fcc metals processed by ECAP at room temperature may be simply scaled by the absolute melting temperature. Furthermore, taking into account the trend of the experimental data obtained over a wide range of grain sizes, it is considered that the characteristic exponent of the Hall–Petch relationship for ultra-fine grained fcc metals is slightly different from the conventional value, indicating an intermediate condition between those of large grains and very fine grains characterized by the activation of totally multi-slip or single slip, respectively, inside the individual grains.

(2) The flow process in the ultrafine-grained materials at low temperatures can be described by steady-state creep, for which grain boundary diffusion becomes a significant factor in determining the rate of steady-state flow. Observations using depth-sensing indentation testing and AFM after ECAP provide unambiguous evidence for the occurrence of grain boundary sliding in pure

aluminum at room temperature. The result is attributed to the introduction of a large number of high-energy non-equilibrium boundaries during processing by ECAP and the consequent excess of extrinsic dislocations in the grain boundaries.

(3) The addition of Mg hinders the annihilation of dislocations in the Al matrix during SPD leading to an increase in the dislocation density, which gives an increase in the dislocation storage capability and therefore in the maximum yield strength of the material. As grain refinement occurs by the re-arrangement of dislocations into dislocation walls and/or grain boundaries, the addition of Mg also decreases the minimum grain size achievable by ECAP.

(4) It is apparent that the yield strengths measured by mechanical testing are in relatively good agreement with the values calculated according to the Taylor equation for different fcc metals and solid solutions processed by SPD, indicating that the strength is basically determined by the interactions between dislocations. At the same time, for precipitation-hardened alloys the strengthening effects include not only the dislocation density but also the role of particle-hardening.

(5) When ECAP is conducted at elevated temperatures, the precipitation processes may be promoted in supersaturated alloys because dislocations act readily as the nucleation sites for precipitates. At the same time, if ECAP is performed on precipitation-hardened alloys the SPD straining may lead to a fragmentation of any rod-like particles. The presence of precipitates stabilizes the ultrafine-grained microstructures at elevated temperatures, thereby enhancing the ability to achieve superplastic ductilities in these alloys.

Acknowledgements The research was supported in part by the Hungarian National Scientific Research Fund, OTKA under Contract Numbers F-047057, T-038048, and T-043247 (NQC and JG) and in part by the National Science Foundation of the United States under Grant No. DMR-024333l (TGL). JG is grateful for the support of a Bolyai János Research Scholarship of the Hungarian Academy of Sciences.

References

1. Hall EO (1951) Proc Phys Soc B64:747
2. Petch NJ (1953) J Iron Steel Inst 174:25
3. Edington JW, Melton KN, Cutler CP (1976) Prog Mater Sci 21:61
4. Langdon TG (1994) Acta Metall Mater 42:2437
5. Chinh NQ, Illy J, Juhász A, Lendvai J (1995) Phys Stat Sol (a) 149:583
6. Nieh TG, Wadsworth J, Sherby OD (1997) Superplasticity in metals, ceramics. Cambridge University Press, Cambridge, UK, p 290
7. Valiev RZ, Estrin Y, Horita Z, Langdon TG, Zehetbauer M, Zhu YT (2006) JOM 58(4):33
8. Iwahashi Y, Wang J, Horita Z, Nemoto M, Langdon TG (1996) Scripta Mater 35:143
9. Iwahashi Y, Horita Z, Nemoto M, Langdon TG (1997) Acta Mater 45:4733
10. Valiev RZ, Islamgaliev RK, Alexandrov IV (2000) Prog Mater Sci 45:103
11. Valiev RZ, Langdon TG (2006) Prog Mater Sci 51:881
12. Iwahashi Y, Horita Z, Nemoto M, Langdon TG (1998) Acta Mater 46:3317
13. Hasegawa H, Komura S, Utsunomiya A, Horita Z, Furukawa M, Nemoto M, Langdon TG (1999) Mater Sci Eng A265:188
14. Komura S, Horita Z, Nemoto M, Langdon TG (1999) J Mater Res 14:4044
15. Vinogradov A, Hashimono S, Patlan V, Kitagawa K (2001) Mater Sci Eng A319–321:862
16. Vinogradov A, Suyuki T, Hashimoto S, Kitagawa K, Kuynetsov A, Dobatkin S (2006) Mater Sci Forum 503–504:971
17. Hadzima B, Janecek M, Hellmig RJ, Kutnyakova Y, Estrin Y (2006) Mater Sci Forum 503–504:883
18. Zhilyaev AP, Gubicza J, Nurislamova G, Révész Á, Suriñach S, Baró MD, Ungár T (2003) Phys Stat Sol (a) 198:263
19. Neishi K, Horita Z, Langdon TG (2002) Mater Sci Eng A325:54
20. Yamashita A, Yamaguchi D, Horita Z, Langdon TG (2000) Mater Sci Eng A287:100
21. Horita Z, Furukawa M, Nemoto M, Barnes AJ, Langdon TG (2000) Acta Mater 48:3633
22. Chinh NQ, Horváth G, Horita Z, Langdon TG (2004) Acta Mater 52:3555
23. Hollomon JH (1945) Trans AIME 162:268
24. Voce E (1948) J Inst Metals 74:537
25. Suzuki T, Vinogradov A, Hashimoto S (2004) Mater Trans 45:2200
26. Wang YM, Ma E, Chen MW (2002) Appl Phys Lett 80:2395
27. Valiev RZ (2004) Nature Mater 3:511
28. Porter DA, Easterling KE (1992) Phase Transformations in Metals and Alloys. 2nd ed., Chapman and Hall, London, UK
29. Schumacher S, Birringer R, Strauss R, Gleiter H (1989) Acta Metall 37:2485
30. Nieman GW, Weertman JR, Siegel RW (1991) J Mater Res 6:1012
31. El-Sherik AM, Erb U, Palumbo G, Aust KT (1992) Scripta Metall Mater 27:1185
32. Weertman JR (1993) Mater Sci Eng A166:161
33. Furukawa M, Horita Z, Nemoto M, Valiev RZ, Langdon TG (1996) Acta Metall 44:4619
34. Meyers MA, Mishra A, Benson DJ (2006) JOM 58(4):41
35. Chokshi AH, Rosen A, Karch J, Gleiter H (1989) Scripta Mater 21:1679
36. Jang JSC, Kock CC (1990) J Mater Res 5:498
37. Liu XD, Hu ZQ, Ding BZ (1992) Nanostruct Mater 2:545
38. Nieh TG, Wadsworth J (1991) Scripta Metall Mater 25:955
39. Scattergood RO, Koch CC (1992) Scripta Metall Mater 27:1195
40. Wang N, Wang Z, Aust KT, Erb U (1997) Mater Sci Eng A237:150
41. Yamakov V, Wolf D, Phillpot SR, Mukherjee AK, Gleiter H (2004) Nature Mater 3:43

42. Kovács I, Zsoldos L (1973) Dislocations and Plastic Deformation. Academy Press, Budapest, Hungary
43. Pande CS, Masumura RA, Armstrong RW (1993) Nanostruct Mater 2:323
44. Mohamed FA, Xun Y (2003) Mater Sci Eng A354:133
45. Dalla Torre F, Lapovok R, Sandlin J, Thomson PF, Davies CHJ, Pereloma EV (2004) Acta Mater 52:4819
46. Zerilli FJ, Armstrong RW (1987) J Appl Phys 61:1816
47. Zehetbauer M, Seumer V (1993) Acta Mater 41:577
48. Zehetbauer M (1993) Acta Mater 41:589
49. Chinh NQ, Illy J, Horita Z, Langdon TG (2005) Mater Sci Eng A410–411:234
50. Chinh NQ, Vörös G, Szommer P, Horita Z, Langdon TG (2006) Mater Sci Forum 503–504:1001
51. Wang YM, Ma E (2004) Mater Sci Eng A375–377:46
52. Xu C, Furukawa M, Horita Z, Langdon TG (2005) Mater Sci Eng A398:66
53. Van Swygenhoven H, Caro A (1997) Appl Phys Lett 71:1652
54. Schiøtz J, Di Tolla FD, Jacobsen KW (1998) Nature 391:561
55. Vinogradov A, Hashimoto S, Patlan V, Kitagawa K (2001) Mater Sci Eng A319–321:862
56. Huang Y, Langdon TG (2003) Mater Sci Eng A358:114
57. Yu CY, Sun PL, Kao PW, Chang CP (2005) Scripta Mater 52:359
58. Chinh NQ, Szommer P, Horita Z, Langdon TG (2006) Adv Mater 18:34
59. Kovács Zs, Chinh NQ, Lendvai J, Horita Z, Langdon TG (2002) Mater Sci Forum 396–402:1073
60. Bérces G, Chinh NQ, Juhász A, Lendvai J (1998) Acta Mater 46:2029
61. Bérces G, Chinh NQ, Juhász A, Lendvai J (1998) J Mater Res 13:1411
62. Chinh NQ, Csikor F, Kovács Zs, Lendvai J (2000) J Mater Res 15:1037
63. Chinh NQ, Horváth Gy, Kovács Zs, Lendvai J (2002) Mater Sci Eng A324:219
64. Chinh NQ, Gubicza J, Kovács Zs, Lendvai J (2004) J Mater Res 19:31
65. Gubicza J, Chinh NQ, Horita Z, Langdon TG (2004) Mater Sci Eng A387–389:55
66. Dubravina A, Zehetbauer MJ, Schafler E, Alexandrov IV (2004) Mater Sci Eng A387:817
67. Gubicza J, Balogh L, Hellmig RJ, Estrin Y, Ungár T (2005) Mater Sci Eng A400–401:334
68. Kuzel R, Matej Z, Cherkaska V, Pesicka J, Cízek J, Procházka I, Islamgaliev RK (2004) J Alloys Comp 378:242
69. Schafler E, Steiner G, Korznikova E, Kerber M, Zehetbauer MJ (2005) Mater Sci Eng A410–411:169
70. Schafler E, Dubravina A, Mingler B, Karnthaler HP, Zehetbauer M (2006) Mater Sci Forum 503–504:51
71. Gubicza J, Chinh NQ, Krállics Gy, Schiller I, Ungár T (2006) Curr Appl Phys 6:194
72. Zhilyaev AP, Gubicza J, Suriñach S, Baró MD, Langdon TG (2003) Mater Sci Forum 426:4507
73. Gubicza J, Krállics Gy, Schiller I, Malgin D (2004) Mater Sci Forum 473–474:453
74. Gubicza J, Schiller I, Chinh NQ, Illy J (2006) Mater Sci Forum 537–538:169
75. Starink MJ, Wang SC (2003) Acta Mater 51:5131
76. Hughes DA, Hansen N (2000) Acta Mater 48:2985
77. Xu C, Dixon W, Furukawa M, Horita Z, Langdon TG (2003) Mater Lett 57:3588
78. Xu C, Furukawa M, Horita Z, Langdon TG (2003) Acta Mater 51:6139
79. Xu C, Furukawa M, Horita Z, Langdon TG (2005) Acta Mater 53:749
80. Xu C, Langdon TG (2005) Mater Sci Eng A410–411:398
81. Xu C, Langdon TG (2006) Mater Sci Forum 503–504:77
82. Kawasaki M, Xu C, Langdon TG (2005) Acta Mater 53:5353
83. Kawasaki M, Xu C, Langdon TG (2006) Mater Sci Forum 503–504:83
84. Lee S, Berbon PB, Furukawa M, Horita Z, Nemoto M, Tsenev NK, Valiev RZ, Langdon TG (1999) Mater Sci Eng A272:63
85. Komura S, Furukawa M, Horita Z, Nemoto M, Langdon TG (2001) Mater Sci Eng A297:111
86. Mckenzie PW, Lapovok R, Thomson PF (2006) Mater Sci Forum 503–504:657
87. Lee S, Utsunomiya A, Akamatsu H, Neishi K, Furukawa M, Horita Z, Langdon TG (2002) Acta Mater 50:553
88. Muruyama M, Horita Z, Hono K (2001) Acta Mater 49:21
89. Zhang Z, Hosoda S, Kim I-S, Watanabe Y (2006) Mater Sci Eng A 425:55
90. Vinogradov A, Patlan V, Suzuki Y, Kitagawa K, Kopylov VI (2002) Acta Mater 50:1639
91. Gao N, Starink MJ, Furukawa M, Horita Z, Xu C, Langdon TG (2006) Mater Sci Forum 503–504:275
92. Zhao YH, Liao XZ, Jin Z, Valiev RZ, Zhu YT (2004) Acta Mater 52:4589
93. Kocks UF (1966) Phil Mag 13:541